Supporting Information

Atomic Ru-Pt dual sites boost mass activity and cycle life of alkaline hydrogen evolution

Yuehuan Zhang and Qiang Yuan*

Experimental section

Chemicals

Chloroplatinic acid ($H_2PtCl_6 \cdot 6H_2O$; 99.9%) was purchased from Aladdin. Ruthenium (III) chloride hydrate ($RuCl_3 \cdot xH_2O$; 99.9%), poly(vinylpyrrolidone) (PVP; K-30, Mw = 30,000), and sodium-dodecyl sulfate ($(C_{12}H_{25}O_4NaS)$, SDS; AR) were purchased from Aldrich. Porous carbon (PC) was purchased from Janpan LlON. 20% Pt/C and 20% Ru/C were purchased from Johnson Matthey and Premetek Company, respectively. IrO_2 was purchased from Alfa-Aesar. All chemicals were used without further purification.

Synthesis of $Ru_{5.67}Pt$/PC：

The catalyst was prepared via the in situ reduction of Ru^{3+} and Pt^{4+} to RuPt alloy nanoclusters on PC. Typically, an aqueous solution of $H_2PtCl_6 \cdot 6H_2O$ (0.01 mmol), an aqueous solution of $RuCl_3.xH_2O$ (0.01 mmol), 65.5 mg of PVP (Mw = 30,000), 60.5 mg of SDS, and 25 mg of PC were dissolved in 15 mL of deionized water and 15 mL of ethanol and stirred for 4 h. The mixed solution was transferred to a Teflon-lined autoclave (50 mL), and the sealed vessel was heated at 150 °C for 3 h. After the product was cooled to room temperature, it was washed several times with deionized water and ethanol via centrifugation at 10,000 rpm for 20 min. The final product was dried under vacuum at 65 °C for 20 h. Additionally, Ru/PC, $Ru_{4.00}Pt$/PC, and $Ru_{3.00}Pt$/PC were synthesized using the same method. $Ru_{4.00}Pt$/PC and $Ru_{3.00}Pt$/PC catalysts were prepared by changing the content of $RuCl_3 \cdot xH_2O$ (0.02 and 0.03 mmol). Inductively

coupled plasma emission spectroscopy (ICP-OES) was used to analyze the composition of the as-prepared RuPt/PC products. The real atomic ratios of Ru:Pt in $Ru_{5.67}Pt$/PC, $Ru_{4.00}Pt$/PC, and $Ru_{3.00}Pt$/PC were 5.67:1, 4.00:1, and 3.00:1, respectively.

Structural characterization

The morphology of the samples was characterized using a Transmission electron microscope (TEM; JEM-1400 Flash at 120 KV) and a double spherical aberration corrected (AC) high angle annular dark-field scanning transmission electron microscope (HAADF-STEM; FEI Spectra 300). The RuPt loading was determined using inductively coupled plasma optical emission spectroscopy (ICP-OES) (Thermo Fisher Scientific, iCAP 7200). The X-ray diffraction (XRD) spectra was performed using a Bruker D8 Advance X-ray powder diffractometer with Cu Kα radiation (λ = 1.5418 Å). X-ray photoelectron spectroscopy (XPS) measurements were obtained using Al Ka X-ray radiation (1,486.6 eV) with an excitation source (Thermo Fisher Scientific, USA). The Brunauer–Emmett–Teller (BET) specific surface area was measured using a Micromeritics ASAP 3020 instrument. XANES and EXAFS data were obtained using BL14W1 crystal monochromators at the Shanghai Synchrotron Radiation Laboratory (SSRF). Pt L_3-edge extended x-ray absorption fine structure (EXAFS) spectra were recorded in the fluorescence mode.

XAFS Analysis and Results

Data reduction, data analysis, and EXAFS fitting were performed and analyzed using the Athena and Artemis programs of the Demeter data analysis packages that utilize the FEFF6 program to fit the EXAFS data.[1, 2] The energy calibration of the sample was conducted using standard Ru foil and Pt foil, which were simultaneously measured as references. A linear function was subtracted from the pre-edge region, and subsequently, the edge jump was normalized using the Athena software. The χ(k) data were isolated by subtracting a smooth, third-order polynomial approximating the absorption background of an isolated atom. The k^3-weighted $\chi(k)$ data were Fourier transformed after applying a Hanning window function (Δk = 1.0). For EXAFS modeling, the global amplitude EXAFS data (*CN, R,* σ^2, and ΔE_0) were obtained by the

nonlinear fitting, with the least-square refinement, of the EXAFS equation to the Fourier-transformed data in *R*-space, using the Artemis software. The EXAFS data of the Ru foil and Pt foil were fitted, and the obtained values of the amplitude reduction factor S_0^2 (0.895 and 0.880) were employed in the EXAFS analysis to determine the coordination numbers (*CNs*) for the Ru-O, Ru-Ru/Pt, Pt-O, and Pt-Ru/Pt scattering path in the sample. For Wavelet Transform analysis, the $\chi(k)$ data exported from Athena were imported into the Hama Fortran code.[3] The parameters are listed as follows: R-range, 1–4 Å; k-range, 0–13 $Å^{-1}$ for sample (for Ru foil, Pt foil, PtO_2, and RuO_2); *k* weight, 2; Morlet function with $\kappa = 6$ and $\sigma = 1$ was used as the mother wavelet to provide the overall distribution.

Electrochemical measurements

Electrochemical measurements were performed using a conventional three-electrode system on a CHI 760e (Chen Hua, Shanghai) electrochemical workstation. In alkaline media, stonewashed rods, Hg/HgO, and catalyst-loaded glassy carbon electrodes (GCE; 5 mm diameter; 0.196 cm^{-2}) were used as counter, reference, and working electrodes, respectively. To prepare the working electrode, 8 mg of the catalyst powder was dispersed in a mixture of 800 μL of ethanol and 200 μL of 5% Nafion and sonicated for 30 min to obtain a homogeneous ink. Thereafter, a specific amount of catalyst ink was dropped onto a GCE with a platinum-group metal loading of 9.6 μg cm^{-2}. The LSV analysis of all the samples was conducted in a solution saturated with hydrogen at a scan rate of 10 mV s^{-1} with IR compensation at 1,600 rpm. Electrochemical impedance spectroscopy was performed in the frequency range of 0.01–100 Hz at an amplitude of 5 mV. The ECSA of the samples was evaluated via CV in the non-Faraday potential window at the scanning rates ranging from 5 to 50 mV s^{-1} based on C_{dl}. For stability testing, the catalyst was dropped onto a carbon paper and evaluated using CV for 50,000 cycles between −200 and 100 mV at a scan rate of 100 mV s^{-1}.

The Tafel slopes of the electrocatalysts were obtained by calculating the polarization curves using the Tafel equation (n = blog(j) + a). All the potentials were referenced to RHE.

The mass activity (MA) reflects the intrinsic activity of the prepared precious metal catalyst and is calculated as follows.

$$\mathrm{MA} = \frac{j}{\mathrm{m}}$$

The TOF is calculated using the following formula.[4]

$$\mathrm{TOF} = \frac{\text{Total Hydrogen Turn Overs Per Geometric area}}{\text{Active Sites Per Geometric area}}$$

The total number of hydrogen turnovers can be obtained from the current density of the polarization curve.

Total Hydrogen Turn Overs:

$$= \left(|j|\frac{\mathrm{mA}}{\mathrm{cm}^2}\right)\left(\frac{1\ \mathrm{C\ s^{-1}}}{1{,}000\ \mathrm{mA}}\right)\left(\frac{1\ \mathrm{mol\ e^-}}{96{,}485.3\ \mathrm{C}}\right)\left(\frac{1\ \mathrm{mol\ H_2}}{2\ \mathrm{mol\ e^-}}\right)\left(\frac{6.022\ \times 10^{23}\ \mathrm{molecules}}{1\ \mathrm{mol\ H_2}}\right)$$

$$= 3.12\ \times 10^{15}|j|\frac{\mathrm{H_2\ (s^{-1})}}{\mathrm{cm}^2}\mathrm{Per}\frac{\mathrm{mA}}{\mathrm{cm}^2}$$

The number of active centers in $Ru_{5.67}Pt/PC$ is calculated from the total mass of Pt at the electrode, assuming that each Pt atom occupies one catalytically active site.

Actives Sites:

$$= \frac{\text{mass loading}\ \times\ \text{catalyst loading per geometric area}\left(\frac{\mathrm{g}}{\mathrm{cm}^2}\right)}{\mathit{P}\mathrm{t\ Mw}\left(\frac{\mathrm{g}}{\mathrm{mol}}\right)}\left(\frac{6.022\ \times 10^{23}\ \mathrm{Pt\ atoms}}{1\ \mathrm{mol\ Pt}}\right)$$

$$= 0.78 \times 10^{16}\ {}_{\text{Pt sites per cm}^2}$$

Therefore, the TOF of $Ru_{5.67}Pt/PC$ can be calculated as follows.

$$\mathrm{TOF} = \frac{3.12\ \times 10^{15}}{0.78\ \times 10^{16}} \times |j|$$

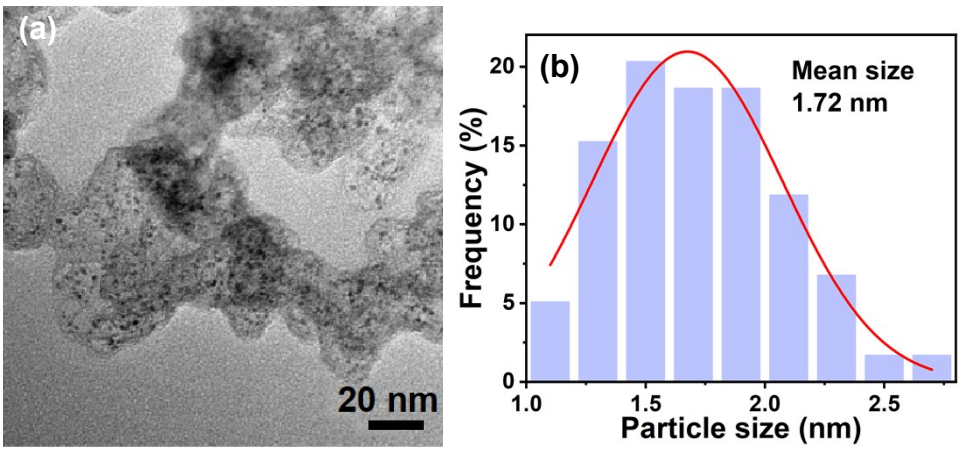

Fig. S1 (a) TEM image and (b) the column chart size of $Ru_{4.00}Pt$/PC.

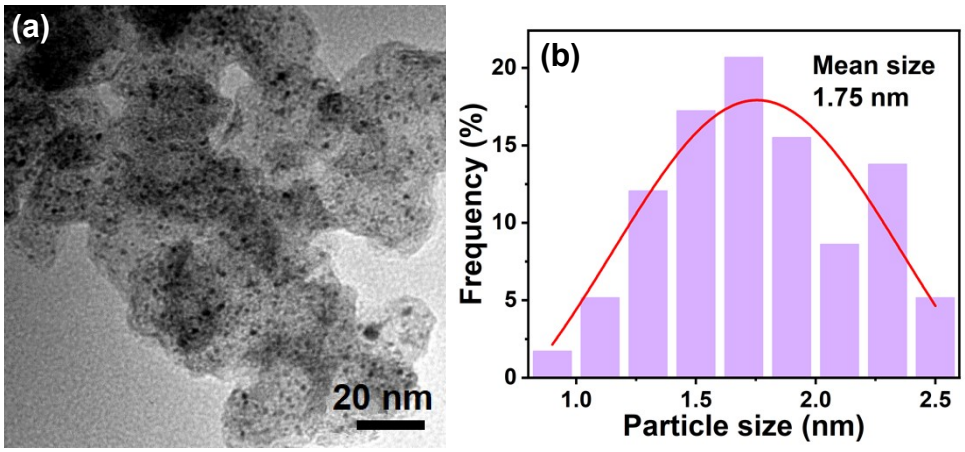

Fig. S2 (a) TEM image and (b) the column chart size of $Ru_{3.00}Pt$/PC.

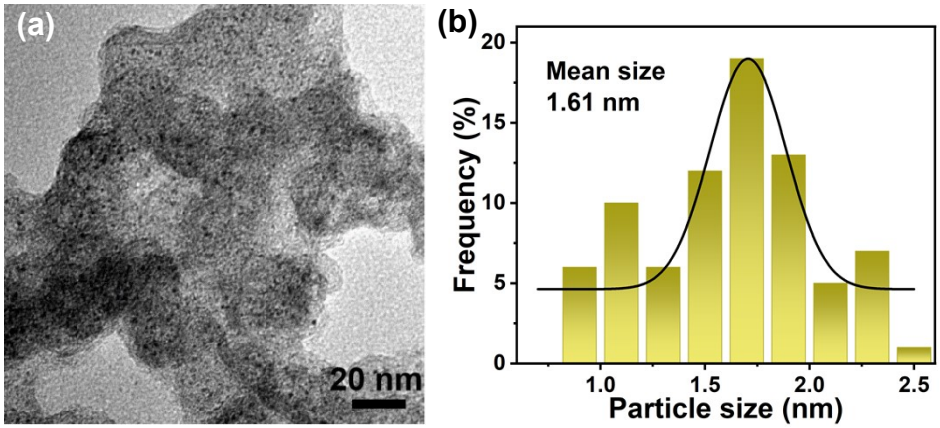

Fig. S3 (a) TEM image and (b) the column chart size of Ru/PC.

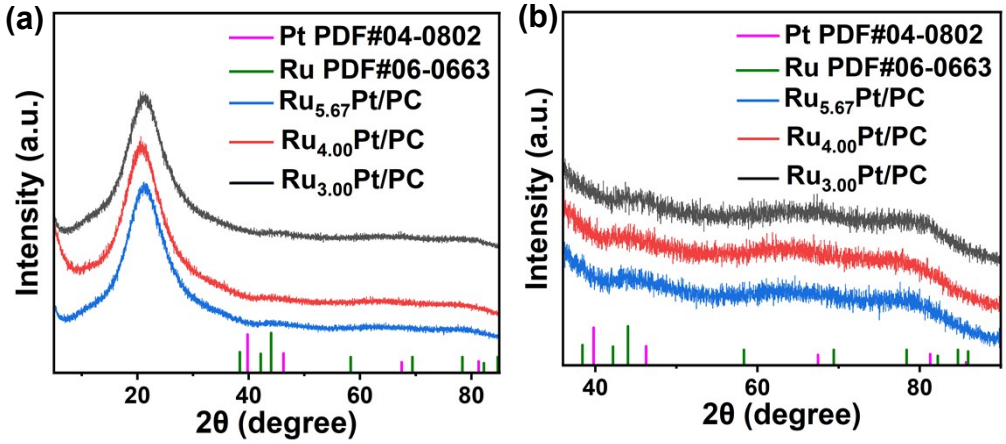

Fig. S4 (a, b) XRD spectra of $Ru_{5.67}Pt/PC$, $Ru_{4.00}Pt/PC$, $Ru_{3.00}Pt/PC$.

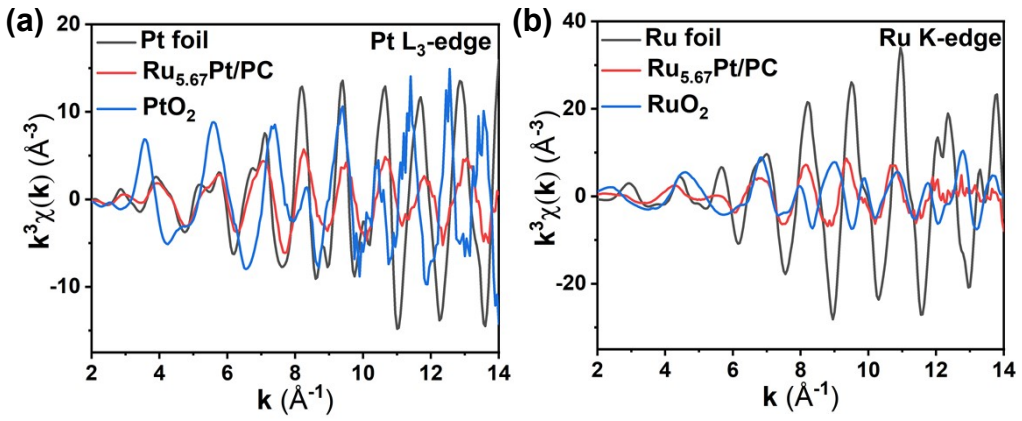

Fig. S5 k^3-weighted spectra at k space of the (a) Pt foil, $Ru_{5.67}Pt/PC$, and PtO_2, and (b) Ru foil, $Ru_{5.67}Pt/PC$, and RuO_2.

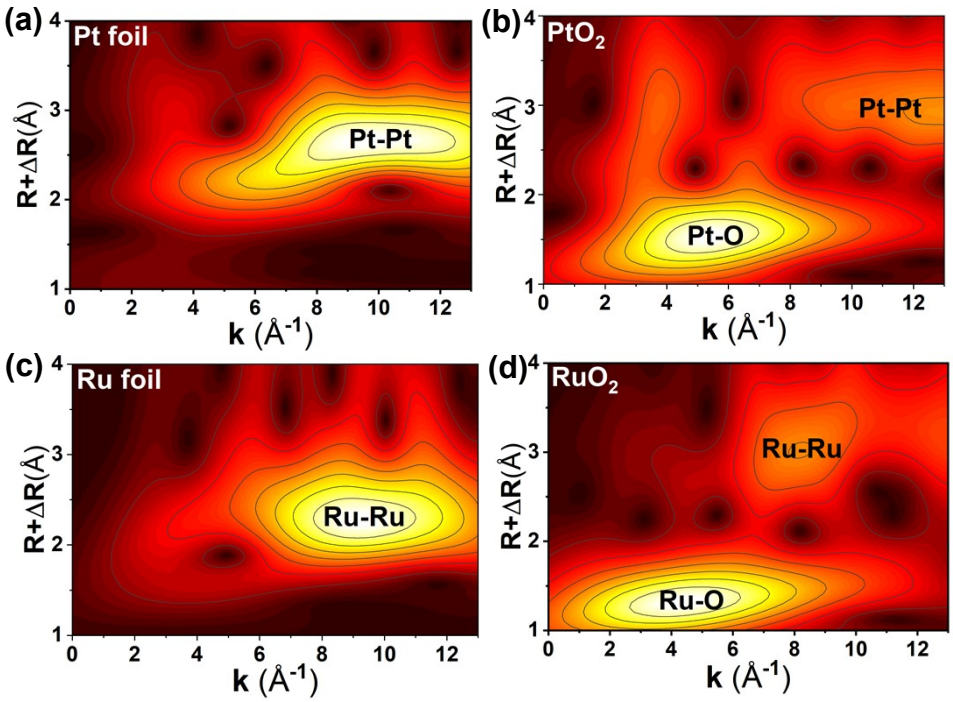

Fig. S6 Wavelet transform maps of (a) Pt foil, (b) PtO_2, (c) Ru foil, and (d) RuO_2.

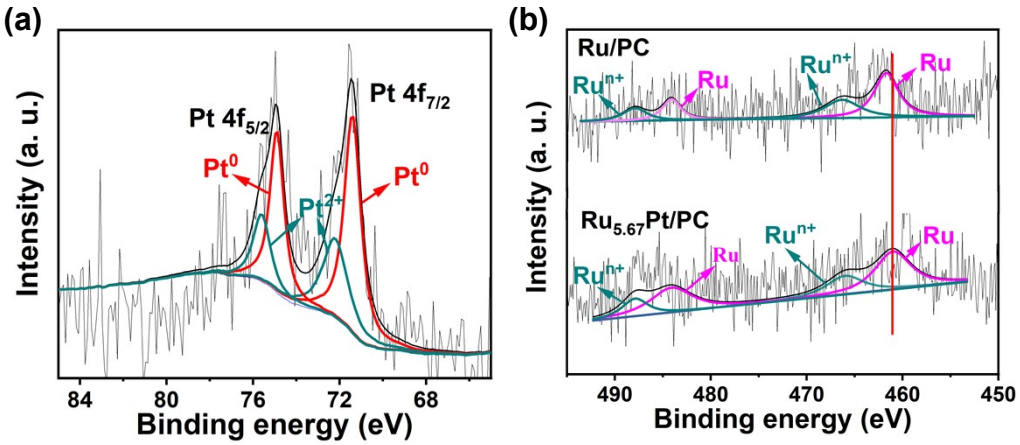

Fig. S7 (a) XPS spectra of Pt 4f for $Ru_{5.67}Pt/PC$. (b) Ru 3p XPS spectra.

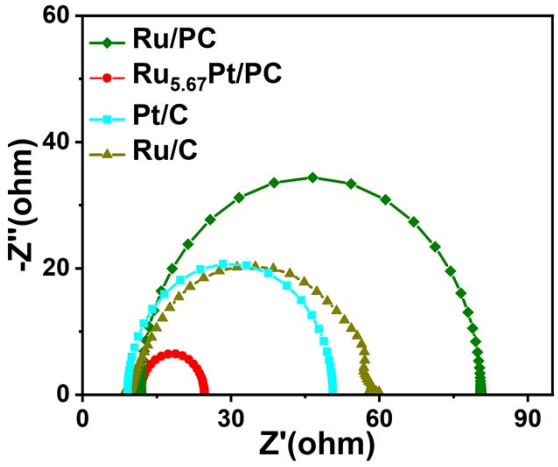

Fig. S8 Nyquist plots of Ru/PC, $Ru_{5.67}Pt/PC$, Pt/C, and Ru/C in 1.0 M KOH.

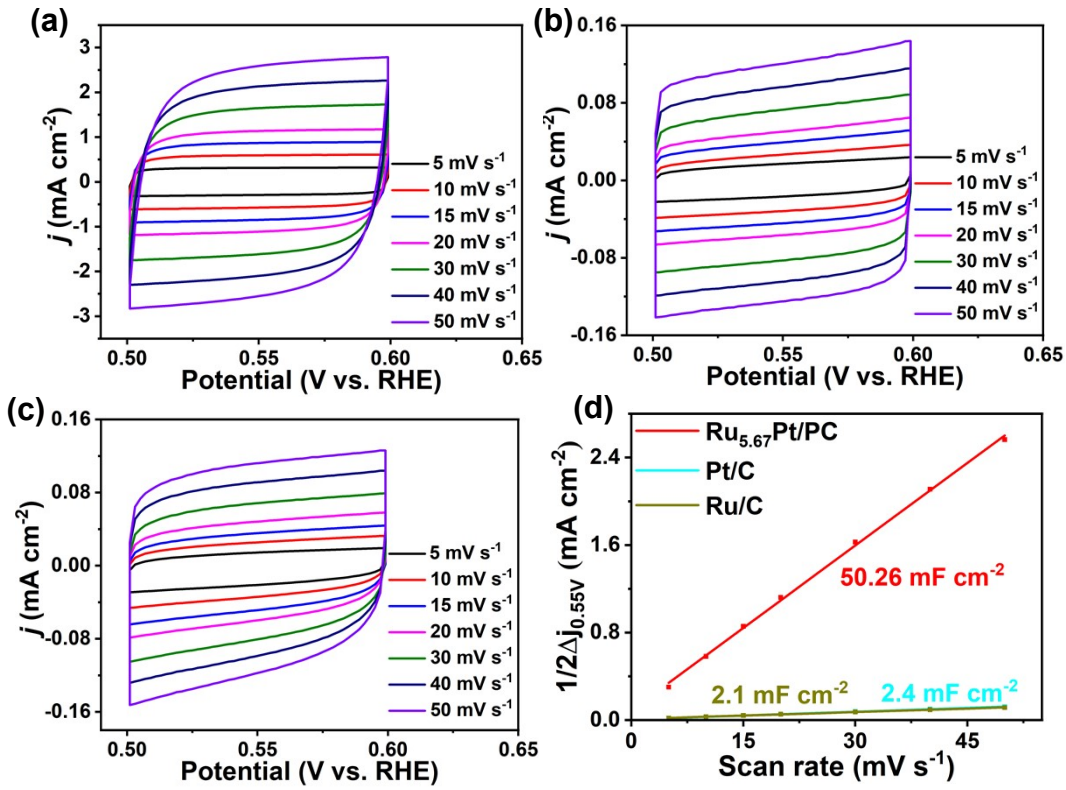

Fig. S9 CV curves with different scan rates from 5 to 50 mV s^{-1} in 1.0 M KOH for (a) $Ru_{5.67}Pt/PC$, (b) Pt/C, and (c) Ru/C. (d) C_{dl} test for $Ru_{5.67}Pt/PC$, Pt/C, and Ru/C.

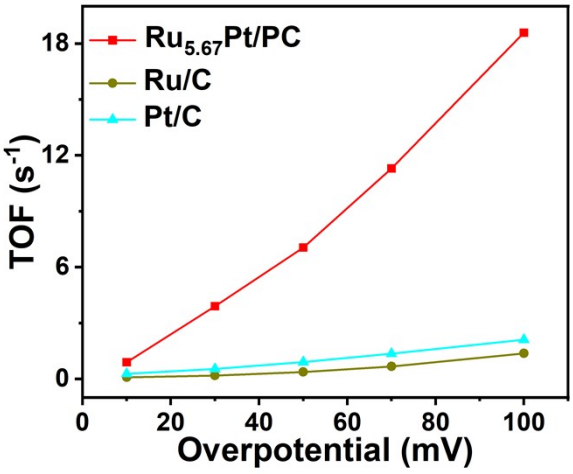

Fig. S10 The TOF curves of $Ru_{5.67}Pt$/PC, Ru/C and Pt/C.

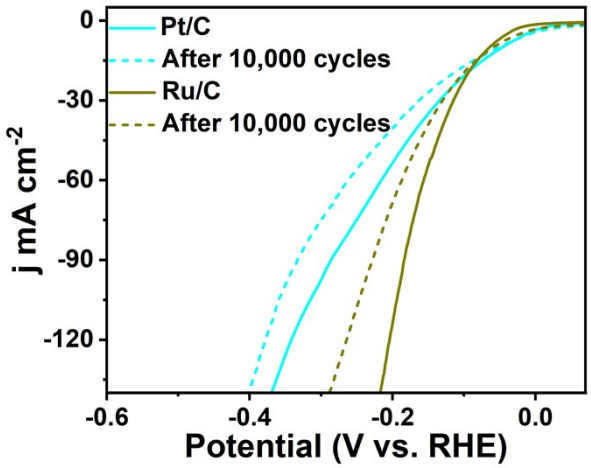

Fig. S11 HER LSV curves of Pt/C and Ru/C before and after 10,000 CV cycles in 1.0 M KOH.

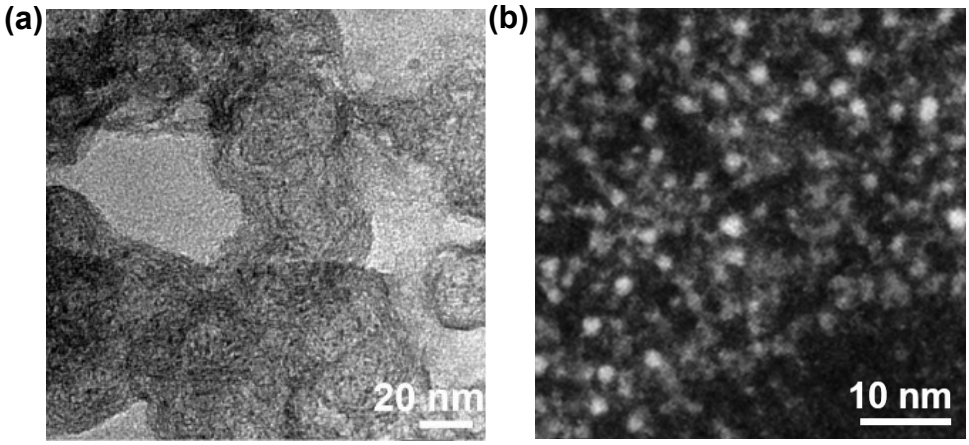

Fig. S12 (a) TEM image, (b) HAADF-STEM image of $Ru_{5.67}Pt$/PC after 50,000 cycles

measurement in 1.0 M KOH.

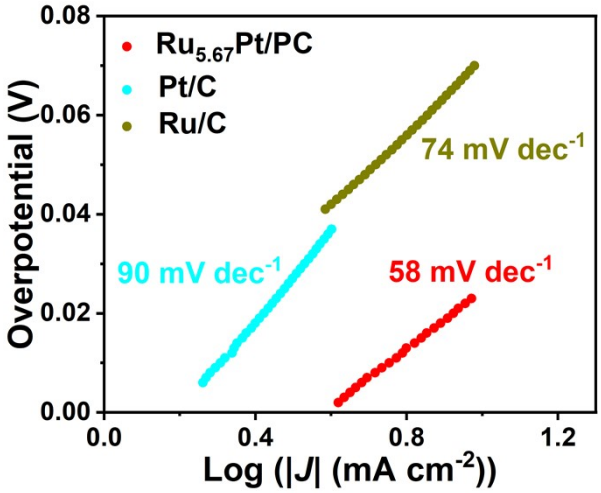

Fig. S13 Tafel plots of $Ru_{5.67}Pt/PC$, Pt/C, and Ru/C in 1.0 M KOH seawater.

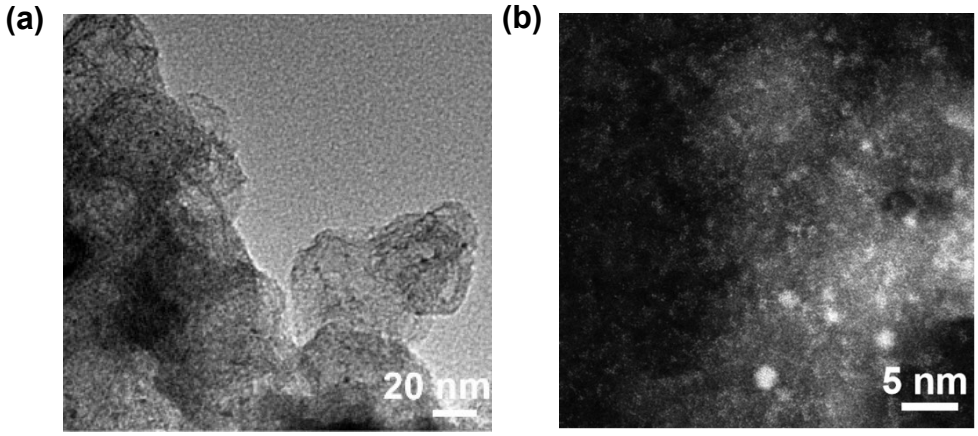

Fig. S14 (a) TEM image, (b) HAADF-STEM image of $Ru_{5.67}Pt/PC$ after 30,000 cycles measurement in 1.0 M KOH seawater.

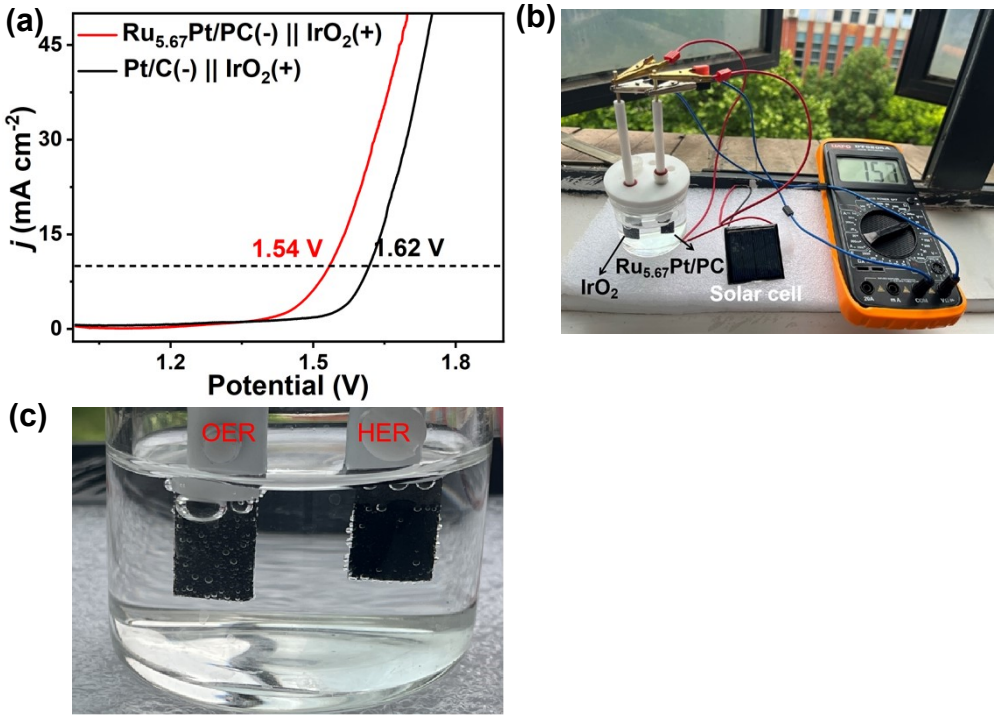

Fig. S15 (a) LSV plots of the IrO_2 || $Ru_{5.67}Pt/PC$ pairs for water splitting in 1.0 M KOH. (b, c) Photo of solar-energy-derived full water splitting and corresponding H_2 and O_2 on carbon cloth.

Table S1. The ICP-OES results for different RuPt nanocatalysts.

Catalysts	Atomic ratios of Ru:Pt	Ru loading (wt.%)	Pt loading (wt.%)	RuPt loading (wt.%)
Ru/PC	-	4.70	-	-
$Ru_{5.67}Pt$/PC	0.85:0.15	2.21	0.80	3.01
$Ru_{4.00}Pt$/PC	0.80:0.20	4.27	2.10	6.37
$Ru_{3.00}Pt$/PC	0.75:0.25	6.63	4.17	10.80

Table S2. EXAFS fitting parameters at the Ru K-edge and Pt L_3-edge for various samples.

Sample	Shell	*CN*[a]	*R*(Å)[b]	σ^2(Å^2)[c]	ΔE_0(eV)[d]	*R* factor
Pt L_3-edge (S_0^2=0.880)						
Pt foil	Pt-Pt	12*	2.757±0.002	0.0050±0.0002	7.3±0.7	0.0025
PtO_2	Pt-O	6.0±0.5	2.024±0.006	0.0033±0.0007	11.3±1.4	0.0074
	Pt-Pt	6.0±0.2	3.091±0.006	0.0100±0.0072	6.9±2.1	
	Pt-O	5.7±0.5	3.697±0.010	0.0033±0.0007	2.7±3.4	
$Ru_{5.67}Pt$ /PC	Pt-O	2.9±0.3	2.141±0.022	0.0033±0.0025	-3.4±0.5	0.0120
	Pt-Ru	2.5±0.3	2.673±0.016	0.0138±0.0022	-3.4±7.9	
	Pt-Pt	7.4±0.4	2.723±0.005	0.0075±0.0008	5.1±1.6	
Ru K-edge (S_0^2=0.895)						
Ru foil	Ru-Ru	12*	2.676±0.002	0.0041±0.0003	-4.7±0.8	0.0044
RuO_2	Ru-O	6.0±0.4	1.976±0.004	0.0032±0.0004	-0.5±1.0	0.0045
	Ru-Ru	3.9±0.5	3.134±0.004	0.0099±0.0013	2.3±1.3	
	Ru-Ru	7.7±0.7	3.576±0.009		-5.0±1.6	
$Ru_{5.67}Pt$ /PC	Ru-O	3.9±0.2	2.002±0.013	0.0060±0.0015	-8.2±3.7	0.0079
	Ru-Ru	4.1±0.4	2.661±0.013	0.0068±0.0023	-8.9±2.5	
	Ru-Pt	2.4±0.6	2.675±0.017	0.0070±0.0048		

[a]*CN*, coordination number; [b]*R*, the distance to the neighboring atom; [c]σ^2, the Mean Square Relative Displacement (MSRD); [d]ΔE_0, inner potential correction; *R* factor indicates the goodness of the fit. S_0^2 was fixed to 0.895 and 0.880, according to the experimental EXAFS fit of Ru foil and Pt foil by fixing *CN* as the known crystallographic value. * This value was fixed during EXAFS fitting, based on the known structure of Ru and Pt. Fitting range: $3.0 \le k$ (/Å) ≤ 13.5 and $1.0 \le R$ (Å) ≤ 3.0 (Ru foil); $3.0 \le k$ (/Å) ≤ 14.0 and $1.0 \le R$ (Å) ≤ 4.0 (RuO_2); $3.0 \le k$ (/Å) ≤ 12.3 and $1.0 \le R$ (Å) ≤ 3.5 (Sample Ru); $3.0 \le k$ (/Å) ≤ 13.8 and $1.0 \le R$ (Å) ≤ 3.0 (Pt foil); $3.0 \le k$ (/Å) ≤ 14.1 and $1.0 \le R$ (Å) ≤ 3.5 (PtO_2); $3.0 \le k$ (/Å) ≤ 13.9 and $1.0 \le R$ (Å) ≤ 4.0

(Sample Pt). A reasonable range of EXAFS fitting parameters: $0.700 < S_0^2 < 1.000$; $CN > 0$; $\sigma^2 > 0$ Å^2; $|\Delta E_0| < 10$ eV; R factor < 0.02.

Table S3. Comparison of various electrocatalysts for HER in 1.0 M KOH electrolyte.

Catalysts	η@10 mA cm^2 (mV vs. RHE)	References
$Ru_{5.67}Pt$/PC	12	This work
RuCo@NC	26	[5]
Ru_1/D-NiFe LDH	18	[6]
PtNi-NC-900	37.4	[7]
Ru@CN	32	[8]
PtNi-O/C	39.8	[9]
Pt-Ru SWNT	46	[10]
Ru-Ni@Ni_2P NRs	31	[11]
RuP_2-CPM	21	[12]
PtRu	15	[13]

Table S4. The comparison of mass activity for $Ru_{5.67}Pt$/PC and the reported catalysts in alkaline condition.

Catalysts	η(mV) @10 mA cm^{-2}	MA@ η(A mg^{-1}_{Pt})	References
$Ru_{5.67}Pt$/PC	12	42.28@70	This work
SANi-PtNWs	-	11.8@70	[14]
PtW NWs/C	18	~4	[15]
NiO_x/Pt_3Ni NWs	40	2.59@70	[16]
Pt/Ni_3S_2/NF	10	5.52@70	[17]
PtNi-O/C	39.8	7.23@70	[9]
Pt_5P_2/a-NiP	9	14.9@70	[18]
N,Pt-MoS_2	38	10.0@70	[19]
Pt_{SA}-$Co(OH)_2$@AgNWS	29	1.6@70	[20]
$Pt/Ni(HCO_3)_2$	27	0.8@70	[21]

Table S5. Comparison of recent reported high-performance Pt-based electrocatalysts for HER in 1.0 M KOH.

Catalysts	η(mV) @10 mA cm^{-2}	Stability	References
$Ru_{5.67}Pt$/PC	12	CV cyclic stability: Stable for 50,000 cycles	This work
Pt-NC/Ni-MOF	25	CV cyclic stability: Stable for 10,000 cycles	[22]
2D-PtND/LDH	25	CV cyclic stability: 8 mV drop (5,000 cycles)	[23]
N-LDH/2D-Pt	31	CV cyclic stability: Stable for 5,000 cycles	[24]
Pt/NiRu-OH	38	CV cyclic stability: 8 mV drop (5,000 cycles)	[25]
PtNi@Ti_3C_2 MXene	36	CV cyclic stability: ~4 mV drop (1,000 cycles)	[26]
Pt-Ni ASs	27.7	CV cyclic stability: Stable for 10,000 cycles	[27]
PtRu	38	CV cyclic stability: Stable for 3,000 cycles	[13]
$PtTe_2$-600 NSs	26	CV cyclic stability: Stable for 20,000 cycles	[28]
Pt-$Ni(OH)_2$/NF	38	CV cyclic stability: Stable for 10,000 cycles	[29]

References

1. S. I. Zabinsky, J. J. Rehr, A. Ankudinov, R. C. Albers and M. J. Eller, *Phys. Rev. B.*, 1995, **52**, 2995-3009.
2. B. Ravel and M. Newville, *J. Synchrotron Radiat*, 2005, **12**, 537-541.
3. H. Funke, M. Chukalina and A. Rossberg, *Phys. Scr.*, 2005, **2005**, 232.
4. K. L. Zhou, Z. Wang, C. B. Han, X. Ke, C. Wang, Y. Jin, Q. Zhang, J. Liu, H. Wang and H. Yan, *Nat. Commun.*, 2021, **12**, 3783.
5. T. Zhu, J. Huang, B. Huang, N. Zhang, S. Liu, Q. Yao, S. C. Haw, Y. C. Chang, C. W. Pao, J. M. Chen, Q. Shao, Z. Hu, Y. Ma and X. Huang, *Adv. Energy Mater.*, 2020, **10**, 2002860.
6. P. Zhai, M. Xia, Y. Wu, G. Zhang, J. Gao, B. Zhang, S. Cao, Y. Zhang, Z. Li, Z. Fan, C. Wang, X. Zhang, J. T. Miller, L. Sun and J. Hou, *Nat. Commun.*, 2021, **12**, 4587.
7. J. Guo, J. Liu, X. Zhang, X. Guan, M. Zeng, J. Shen, J. Zou, Q. Chen, T. Wang and D. Qian, *J. Mater. Chem. A*, 2022, **10**, 13727-13734.
8. J. Wang, Z. Wei, S. Mao, H. Li and Y. Wang, *Energy Environ. Sci.*, 2018, **11**, 800-806.
9. Z. Zhao, H. Liu, W. Gao, W. Xue, Z. Liu, J. Huang, X. Pan and Y. Huang, *J. Am. Chem. Soc.*, 2018, **140**, 9046-9050.
10. F. S. M. Ali, R. L. Arevalo, M. Vandichel, F. Speck, E. L. Rautama, H. Jiang, O. Sorsa, K. Mustonen, S. Cherevko and T. Kallio, *Appl. Catal. B: Environ.*, 2022, **315**, 121541.
11. Y. Liu, S. Liu, Y. Wang, Q. Zhang, L. Gu, S. Zhao, D. Xu, Y. Li, J. Bao and Z. Dai, *J. Am. Chem. Soc.*, 2018, **140**, 2731-2734.
12. Y. Li, J. Zhang, Y. Liu, Q. Qian, Z. Li, Y. Zhu and G. Zhang, *Sci. Adv.*, 2020, **6**, eabb4197.
13. B. Pang, X. Liu, T. Liu, T. Chen, X. Shen, W. Zhang, S. Wang, T. Liu, D. Liu, T. Ding, Z. Liao, Y. Li, C. Liang and T. Yao, *Energy Environ. Sci.*, 2022, **15**, 102-108.
14. M. Li, K. Duanmu, C. Wan, T. Cheng, L. Zhang, S. Dai, W. Chen, Z. Zhao, P. Li, H. Fei, Y. Zhu, R. Yu, J. Luo, K. Zang, Z. Lin, M. Ding, J. Huang, H. Sun, J. Guo, X. Pan, W. A. Goddard, P. Sautet, Y. Huang and X. Duan, *Nat. Catal.*, 2019, **2**, 495-503.
15. L. Gao, Z. Yang, T. Sun, X. Tan, W. Lai, M. Li, J. Kim, Y. F. Lu, S. I. Choi, W. Zhang, C. Ma, S. C. Smith, Y. G. Zhou and H. Huang, *Adv. Energy Mater.,* 2022, **12**, 2103943.
16. P. Wang, K. Jiang, G. Wang, J. Yao and X. Huang, *Angew. Chem. Int. Edit.*, 2016, **55**, 12859-12863.
17. Z. Xing, D. Wang, T. Meng and X. Yang, *ACS Appl. Mater. Inter.*, 2020, **12**, 39163-39169.

18. Y. Li, Z. Wu, X. Zhang, F. Song, L. Cao, H. Sheng, X. Gao, C. Li, H. Li, W. Li and B. Dong, *Small*, 2023, **19**, 2206859.
19. Y. Sun, Y. Zang, W. Tian, X. Yu, J. Qi, L. Chen, X. Liu and H. Qiu, *Energy Environ. Sci.*, 2022, **15**, 1201-1210.
20. K. L. Zhou, C. Wang, Z. Wang, C. B. Han, Q. Zhang, X. Ke, J. Liu and H. Wang, *Energy Environ. Sci.*, 2020, **13**, 3082-3092.
21. M. Lao, K. Rui, G. Zhao, P. Cui, X. Zheng, S. X. Dou and W. Sun, *Angew. Chem. Int. Edit.*, 2019, **58**, 5432-5437.
22. C. Guo, Y. Jiao, Y. Zheng, J. Luo, K. Davey and S. Z. Qiao, *Chem.*, 2019, **5**, 2429-2441.
23. Y. R. Hong, S. Dutta, S. W. Jang, O. F. Ngome Okello, H. Im, S. Y. Choi, J. W. Han and I. S. Lee, *J. Am. Chem. Soc.*, 2022, **144**, 9033-9043.
24. S. W. Jang, S. Dutta, A. Kumar, Y. R. Hong, H. Kang, S. Lee, S. Ryu, W. Choi and I. S. Lee, *ACS Nano*, 2020, **14**, 10578-10588.
25. D. Li, X. Chen, Y. Lv, G. Zhang, Y. Huang, W. Liu, Y. Li, R. Chen, C. Nuckolls and H. Ni, *Appl. Catal. B: Environ.*, 2020, **269**, 118824.
26. Y. Yan, R. Zhang, Y. Yu, Z. Sun, R. Che, B. Wei, A. P. LaGrow, Z. Wang and W. Zhou, *Appl. Catal. B: Environ.*, 2021, **291**, 120100.
27. Z. Zhang, G. Liu, X. Cui, B. Chen, Y. Zhu, Y. Gong, F. Saleem, S. Xi, Y. Du, A. Borgna, Z. Lai, Q. Zhang, B. Li, Y. Zong, Y. Han, L. Gu and H. Zhang, *Adv. Mater.*, 2018, **30**, 1801741.
28. X. Li, Y. Fang, J. Wang, H. Fang, S. Xi, X. Zhao, D. Xu, H. Xu, W. Yu, X. Hai, C. Chen, C. Yao, H. B. Tao, A. G. R. Howe, S. J. Pennycook, B. Liu, J. Lu and C. Su, *Nat. Commun.*, 2021, **12**, 2351.
29. G. Yuan, B. Wen, Y. Hu, G. Zeng, W. Zhang, L. Wang, X. Zhang and Q. Wang, *Int. J. Hydrogen Energy*, 2019, **44**, 14258-14265.